EXPERIMENTAL AND NUMERICAL INVESTIGATION OF SHAPE MEMORY ALLOY HYBRID COMPOSITES WITH ELASTOMERIC INTERFACE

G. Pisaneschi[1*], T. M. Brugo[1], P. Cosseddu[1], G. Scalet[2], and A. Zucchelli[1]

[1] Department of Industrial Engineering (DIN), University of Bologna, Bologna, Italy
[2] Department of Civil Engineering and Architecture (DICAr), University of Pavia, Italy
* Corresponding author (gregorio.pisaneschi@unibo.it)

Keywords: Shape Memory Alloy, Composite, Elastomer, Adhesion, Cohesive Zone Model

ABSTRACT

Shape memory alloy (SMA) in hybrid composites (SMAHC) have been extensively studied for their ability to tune composite proprieties. SMA can exhibit pseudo elasticity and shape memory effect, which can improve the performance of composites or change their original shape, for instance.

However, these effects depend on the ability of the SMA to undergo martensitic phase transformation (MPT) under high strains and stresses. Previous studies have shown that the SMA wires embedded in a composite matrix tend to debond at the interfaces when MPT occurs, reducing the effectiveness of the SMA. Therefore, improving the interfacial adhesion between the SMA and the matrix is a crucial challenge for SMAHC.

One possible way to improve the interfacial adhesion is to introduce a thin layer of a rubber-like elastomer (KRAIBON®) between the SMA and the matrix. This approach has been successfully applied in metal-CFRP interfaces, where the rubber-like layer reduced the residual stresses during curing and increased the fracture toughness. In this work, we investigated the effect of the elastomeric interface on the bonding behaviour of SMA wires embedded in a composite matrix.

We fabricated and tested pull-out specimens of one length with SMA SE wires interfaced with either epoxy or KRAIBON®. We found that the specimens with the elastomer showed higher bond strength and delayed debonding than those with epoxy. The rubber-like layer allowed the MPT, resulting in higher force transfer and energy dissipation.

To further understand the debonding mechanism, we developed a 3-D finite element model (FEM) with a cohesive zone model (CZM) to simulate the pull-out test. The FEM results agreed with the experimental data and provided insights into the stress distribution and damage evolution.

This work demonstrates the potential of using an elastomer as an interfacial material for SMAHC, which could improve self-actuated composites for morphing applications.

1 INTRODUCTION

Shape memory alloys (SMAs) have gained popularity in various engineering domains due to their remarkable properties of recovering their original shape after undergoing large deformations. As SMAs are increasingly used in different engineering applications, there is also a growing interest in developing SMA composites that can exploit or complement the performance of SMAs.

In particular, SMA hybrid composites (SMAHCs) are polymer matrix composites (lamina or laminates of fibre-reinforced polymers) reinforced by SMA wires or ribbons. SMAHCs combine the properties of conventional composites with the Shape Memory Effect (SME) and Pseudo-elasticity (PE) of SMAs aiming to enhance or modify performances or related characteristics.

SME of SMA wires was initially used to actively tune the proprieties of the SMAHC for damping and vibration [1]. Early investigations included improved impact damage resistance via the dissipative nature of the hysteric response of pseudo-elastic SMAs [2]. Shape morphing was considered a promising candidate for the geometry modification of structures. Chaudhry and Rogers first analysed composite actuators in the form of a beam[3]. These features make them attractive for various engineering applications, especially aerospace and automotive.

However, the development of SMAHC faces many challenges, such as processing methods, interface bonding, mechanical behaviour, and modelling techniques. Therefore, various research efforts have been devoted to exploring the potential of SMA composites and improving their performance-related characteristics by optimising their design, fabrication, and testing [4].

One of the challenges in designing SMAHCs is to ensure good interfacial adhesion between the SMA elements and the matrix or reinforcement materials. A poor interface can lead to premature failure, reduced load transfer, and diminished shape memory effects. Therefore, various methods have been proposed to improve the interfacial adhesion, such as surface treatments or functionalisation, mechanical interlocking, or chemical bonding and pull-out experiments were performed to characterise the strength and energy of the cohesive interface ([5]–[8]).

Payandeh et al. [9] concluded that the bonded part of wires with SME could not undergo martensitic phase transformation (MPT) since the latter induces considerable deformation and, thus, significant shear stresses, leading to debonding at the epoxy interfaces. The same result was obtained for SE wires by Dawood et al. [10]. According to Antico et al. simulations [8], the debonding front had wire thinning that resulted in significant, cohesive energy for mode I (i.e., when normal opening displacement is applied to the interface) contribution respect *mode II* (only shear), reducing the pull-out forces during debonding.

2 RESEARCH SIGNIFICANCE

The initial aim of this research was to develop a shape-morphing flap that could enhance the braking performance of an electric motorcycle. This flap is a SMAHC, which can change its shape in response to temperature changes, thanks to the heat of the joule effect. One example of GFRP application is in the study by Min-Woo et al., where they combined glass fibres with SMA wires to create a smart soft composite; the SMAHC was attached to the rear spoiler of a car to enhance its aerodynamic performance [11]. This example and other designs exist in the literature, but manufacturing such a flap is challenging, especially considering the interface adhesion problems during the martensite transformation mentioned above.

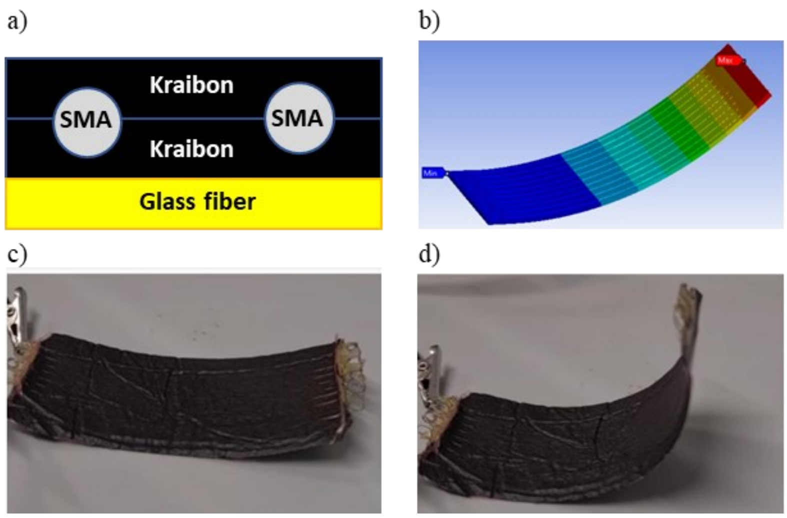

Figure1: a) lamination sequence, b) FEM of actuated SMAHC,
c) laminated SMAHC, d) SMAHC actuated by joule effect.

Therefore, our study proposes a novel method to fabricate SMAHCs with an elastomeric interface (KRAIBON®) that can provide a flexible and durable connection between the SMA elements and the matrix. KRAIBON® is a thin film of rubber-like elastomer that can be co-cured with epoxy resin without additional adhesive. In the investigation of Povolo et al. [12], this approach avoided the problems associated with residual stresses that develop during the curing process by reducing the stress peaks thanks to the deformable behaviour of the interface. In the case of the SMAHC, the main advantage of using KRAIBON® is that it can reduce the residual stresses and accommodate the large deformations induced by the SMA fibres during phase transformation, thus preventing debonding and improving the mechanical performance of SMAHCs without requiring any special treatments.

First, we tested the concept of integration in a laminate using KRAIBON ® as an interface. It can be seen the stacking sequence (Fig. 1a) and the Finite Element Model (FEM) of the actuated laminate (Fig. 1b), in which was used the Turner model for the SME [13]. Then we proceeded with the experiment. We used a single SME wire of 0.2 mm diameter and 90 °C of Austenite starting (As) temperature. The results of the cured and the actuated laminate (Fig. 1 c, d) surpassed our expectations. Thus, we proceeded with an experimental campaign to analyse the interfacial adhesion.

Then, we investigated experimentally the interfacial adhesion of SMA wire embedded in Glass Fibre Reinforced Polymer (GFRP) specimens by pull-out tests, comparing the results of specimens with or without the elastomeric interface. Thus, we proposed some FEMs, which included cohesive elements, to address several issues related to the material behaviour and the numerical model. The FEMs were then validated by experimental tests. Finally, we used the numerical results to investigate the stress distributions and deformation mechanisms of the SMAHCs.

3 EXPERIMENTAL CAMPAIGNS

3.1 Specimens and tests setup

We conducted a preliminary test to examine the optimal length of the SMA wire embedded in GFRP and KRAIBON® specimens. We used a pseud-elastic wire without heating to simulate the most critical case (i.e. when all SMA is in the Austenite phase). We also chose a length that allowed the martensite transformation within the matrix and compared the performance of the two specimens under large strain. We produced the specimens using a hand lay-up method (Fig. 2a, 2b, 2c). The plies were placed and

a) b) c) d)

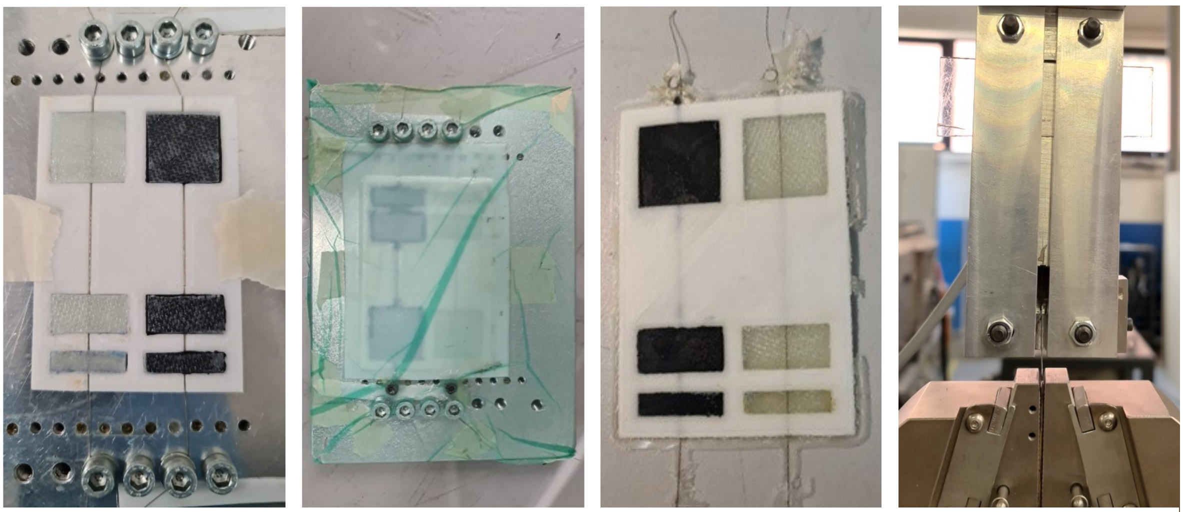

Figure 2: a) stacking sequence with the fixture, b) front of the cured specimens wrapped up in the vacuum bag, c) rear of the cured specimens, d) specimens mounted for pull-out testing.

contained with a 3D-printed fixture. For the fixture, we chose a material that could overcome the curing temperature, avoid stickiness with the matrix, and easily separate from the specimens. The fixture also helped to centre the wire and to create specimens of the desired size. A sheet of PTFE was used to cover the plies and fixture to aid the correct levelling of the material during the curing and to avoid sticking to the vacuum bag. Curing was performed in an autoclave with 3 bars of pressure and 1 bar acting in the vacuum bag. We produced pull-out test specimens embedding SMA filaments in a prismatic composite laminate 20 mm wide with three lengths, 1/4, 1/2 and 1 inch, each corresponding to a bonding length. Two stacking sequences were considered to manufacture the prismatic composite laminate, one with KRAIBON® (KR) and one with an epoxy (EP) interface. The sequences and curing cycles were:

Specimens EP) 3 plies of GFRP + SE SMA wire + 3 Ply of GFRP,
60 minutes at 120 °C (heating ramp: 2 °C/min).

Specimens KR) 1 ply GFRP + 1 ply KRAIBON® + SE SMA wire + 1 ply KRAIBON® + 1 ply GFRP,
15 minutes at 150 °C (heating ramp: 2 °C/min).

These specimens were preliminarily investigated by pull-out test to evaluate the most suitable embedding length that enables the martensitic transformation. From these preliminary tests, we chose 1/2" (12.7 mm) of the embedding length of the SMA wire in the composite laminate for further investigation. Using the same method, we produced four pull-out test specimens of dimension 20 × 12.7 mm for each stacking sequence (specimens KR and EP). We tested three repetitions for each configuration. We used an Instron 8033 servo-hydraulic universal testing machine with a 2 kN load cell and set a constant displacement rate with a 2 mm/min speed. A custom-made gripper system held the laminate specimen (Fig. 2d). It was made to compress the laminate at the sides, block it, and leave a central window of 5 mm to avoid compression over the wire and to see the specimen. On the other side, an Instron mechanical wedge action grip held the free wire. The free wire length was 50 mm, the same for all the specimens, and fixed in the gripper at 26.5 mm from the edge of the laminate to avoid a different elastic behaviour during the pull-out tests.

3.2 Materials

The wire from SAES® is a High Strength SE Ni:Ti wire with a nominal composition by weight of 55.8±0.5% nickel, titanium balanced, O, Fe, and C, all under 0.05 %. It has a diameter of 0.2 mm and a light oxide surface (also known as amber). The As temperature is equal to -25 ± 12 °C and Af (austenite finish) temperature is equal to -8 ± 16 °C, both measured by DSC as reported by the manufacturer. Tensile tests were carried out for the SMA wire with the same machine, with a crimped wire, 100 mm long, held by both sides with the Instron mechanical wedge action grip. The wire was loaded under displacement control at 1 mm/min monolithically until failure. The stress-strain curve of one of the tests is shown in Fig. 3. The Young modulus is 64.8 GPa, and the upper plateau stress is 543 MPa.

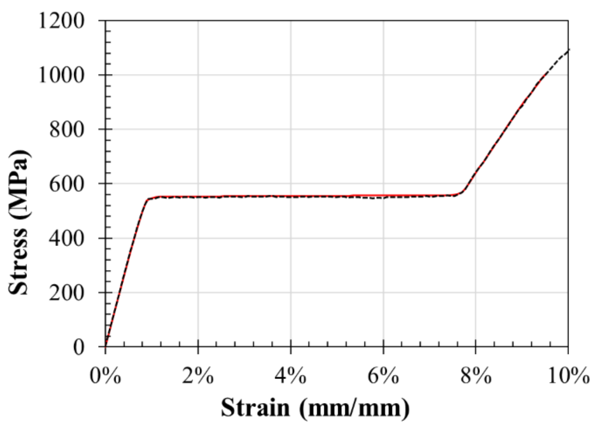

Figure 3: Stress-strain curve of SMA wire test (dotted line), compared with the FEM curve (red line).

The GFRP used in this research is a 0.22 mm thick prepreg (E-glass 8H Satin 300 g/m2 epoxy matrix, VV300S - DT121H-34 Delta-Preg). According to the manufacturer datasheet, the Young modulus is 20 GPa, the Poisson coefficient is 0.13, and the shear modulus is 4.2 GPa.

The elastomer used in this study is KRAIBON®, supplied by Gummiwerk KRAIBURG GmbH & Co. KG. It is a product designed to be co-cured with thermosetting resin to bond metals and composites together. We used the AA6CFZ, with an average thickness of 0.5 mm. The properties provided by the manufacturer were acquired with tensile tests according to DIN 54504: Young modulus of 8.53 GPa, the tensile strength of 4.5 MPa and Poisson coefficient of 0.42.

3.3 Results

All the specimens tested by pull-out failed by complete debonding. Differences in the maximum force can be observed due to different ways of debonding. Tab. 1 reports the results obtained from the force-displacement curves. In Fig. 4, as an example, the graph of two specimens, KR and EP, is shown.

In specimen EP, Fig. 4a, the MPT starts within the free wire (+) at around 17 N and continues until its completion (×) at around 18 N. At this point, the transformation starts within the embedded wire, and the force slightly increases. At the same time, due to the large deformation, the debonding process begins (+) and follows the MPT propagation until the complete detachment of the wire (×) at around 20 N (corresponding to 640 MPa of stress in the wire). The progression was directly observed thanks to the transparency of the GFRP and shown in Fig. 4c.

In specimen KR, Fig. 4b, the transformation starts around the same force (+) but at a more significant displacement due to the more compliant matrix. When the free part of the SMA wire is completely transformed (×), the embedded part starts to change the phase. Contrary to what happens in specimen EP, in specimen KR, thanks to the elastomeric interface, the wire remains attached to the matrix despite the large deformation and the force increase until the debonding (+) begins at around 28 N of force (corresponding to 890 MPa in the wire). In this case, it follows a quick degradation of the adhesion and a fast progression until the complete detachment of the wire (×).

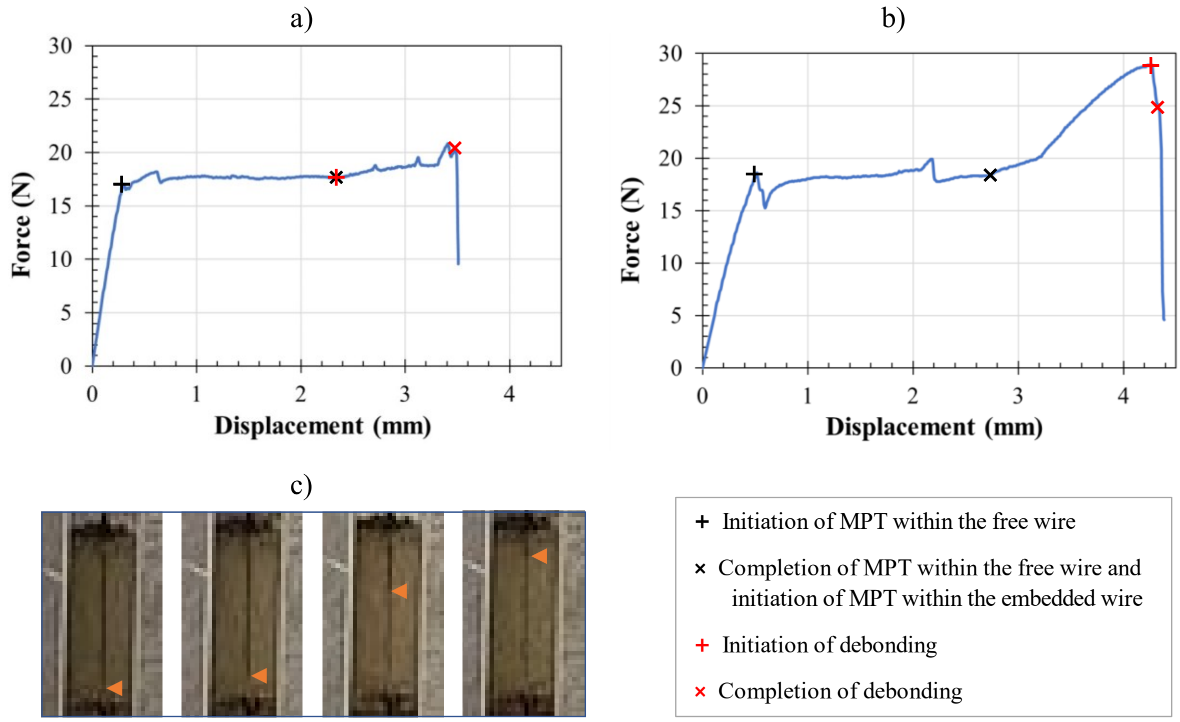

Figure 4: Force-displacement for specimen a) with epoxy interface EP, and b) with elastomeric interface KR; c) progression of the debonding in the specimen EP.

	Maximum Force (MPa)	*τ average @ Max. F.* (MPa)	*Total Energy* (KJ)
Specimen EP	20.33 ± 0.56	2.548 ± 0.070	61.57 ± 1.65
Specimen KR	28.42 ± 0.76	3.562 ± 0.095	80.40 ± 4.09

Table 1: Results of the pull-out tests.

4 NUMERICAL ANALYSES

We developed a finite element analysis (FEA) with non-linear material properties in ANSYS Workbench Mechanical to simulate the pull-out tests. First, a model with shared nodes at the interface was used to study the specimen's stress and strain distribution and get initial values for the cohesive zone model (CZM). Then a design of experiment (DOE) with an interface modelled by CZM was performed to find the correct parameters to represent what we observed in the experiments for specimens KR and EP.

4.1 Finite element model

The geometry was modelled in axisymmetric coordinates to reduce the high computational time of the non-linear simulations. The FEM model geometry, the boundary conditions and the path along the interface (P1-P2), where stresses and deformations were then calculated, are illustrated in Fig. 5.
In addition, only the part of the specimen not gripped by the clamps—precisely, the free wire's 26.5 mm length and the free composite's 5 mm window—was modelled. We applied a fixed constraint to one side of the specimen while there was a controlled displacement at the free wire end.

We created material models using data from manufacturer datasheets and experimental tests. Specifically, we created the SMA wire's multilinear model using the results of tensile tests. In Fig. 3, a comparison of the FEM simulation result and the experimental results is shown. The GFRP was modelled with the orthotropic model for GFRP already available in ANSYS but with datasheet values. Finally, for the KRAIBON®, a Moolin-Rivlin hyperelastic material was also modelled from the manufacturer data of a tensile test.

For the simulation of specimen EP, we used a mesh with axisymmetric linear elements (PLANE182). For specimen KR, we used a mesh with axisymmetric quadratic elements (PLANE183) to overcome convergence issues due to the large deformation of the matrix.

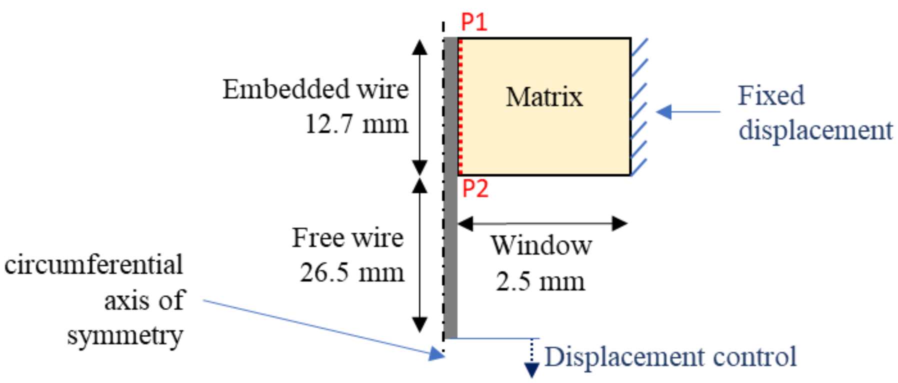

Figure 5: FEM geometry, boundary conditions and interface path (P1-P2).

4.2 Cohesive zone model

The CZM can simulate how cracks propagate in a material: it uses a fictitious contact element with strength and stiffness properties to represent the interface between two materials. These characteristics enable the model to depict the behaviour of the adhesive force acting at the interface and preventing fracture onset. Once the crack starts to propagate, the model also describes the stiffness of the interface degradation as the adhesive force reaches its maximum value and the detachment is complete.

This study employs interface elements defined by the displacement jump, that is, the difference in displacement between two adjacent surfaces at the interface [14]. In *mode I* and *mode II*, the separation of the material interfaces is dominated by the displacement jump, respectively, normal and tangent to the interface. We chose a bilinear CZM model that can be used with interface elements. It simulates mixed behaviour at the interface with both *mode I* and *mode II* stresses. This model is based on traction-separation law in which the variables are the normal and tangential stresses (σ, τ) and the relative displacements (δ_n, δ_t). For both modes, the energy dissipated due to failure, G_n and G_t, can be calculated, and a combined energy criterion is used to define debonding completion.

CZM traction law parameters were obtained starting from bulky preliminary simulations (without CZM) and then optimised by performing DOEs on the CZM simulation to fit the experimental results. Thus, we ran bulky simulations with shared topology at the interface, reaching forces levels comparable to those measured experimentally before the debonding. These simulations helped us to obtain the tentative values of τ and σ at the interface used to model the DOE of the cohesive elements. These values are calculated as average values in the path at the interface (Fig. 5), while the displacements (δ_n, δ_t) are those related to the last node at the interface since it is the most deformed in the structure. The large deflection was turned on in analysis settings for these simulations due to the significant strain of the SMA wire and the elastomer.

This preliminary analysis showed that in the case of KRAIBON® *mode I* stress is negligible compared to *mode II*. As expected, in the case of the resin interface ([8], [10], [15]) *mode I* and *mode II* energy values are comparable. Instead, in the case of the elastomeric interface *mode I* has about two orders of magnitude lower energy than *mode II* (Tab. 2). In specimen EP, the shear stress was about 18 MPa, and the relative displacement was 0.04 mm. The normal stress was 8 MPa, and the relative displacement was 0.04 mm. The MPT of the free wire starts from the side of the wedge gripper. Once it reaches the wire embedded in the matrix, the stress rises, concentrated around that point at the beginning of the interface, as shown in Fig.6.

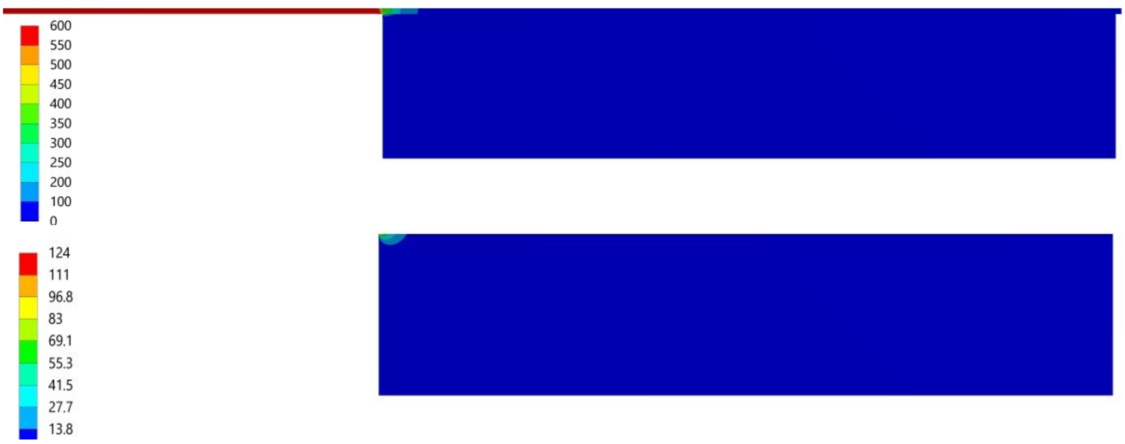

Figure 6: Specimen EP, in the image above the Equivalent Von-Mises stress distribution, in the image below the shear stress in the matrix (values in the scale are in MPa).

Figure 7: Specimen KR, in the image above the Equivalent Von-Mises stress distribution, in the image below the shear stress in the matrix (values in the scale are in MPa).

For Specimen KR, shear stress was 5.75 MPa, lower than the EP, but the displacements were larger, 0.87 mm, leading to more matrix deformation and stress redistribution, as shown in Fig. 7. We assumed that *mode I* did not contribute to debonding in specimen KR and we chose a higher tentative value. We set the initial CZM model with a normal stress of 7 MPa and a normal displacement of 0.01 mm. This setting gives a normal stress of 3.5 MPa at a displacement of 0.004 mm. To accurately simulate the KRAIBON® behaviour, a *mode I* characterisation by DCB testing is needed, but this is not required for Pull-Out simulations because *mode II* failure usually occurs and *mode I* contribution is negligible.

4.3 Optimisation and Validation of the cohesive zone model

We investigated the effect of large deflection on the results of the simulations with CZM. We found that enabling large deflection did not significantly alter the stress and strain distributions but increased the computational cost considerably. Therefore, the large deflection option was turned off for the simulations with the CZM to improve the efficiency of the analysis. All solution settings were *Program Controlled*, except for the *Stabilisation* (*Energy method*, *Constant*, *Energy dissipation* equal to 10^{-4}) to facilitate convergence at the time of detachment of cohesive elements and thus the rigid motion of the wire. We performed a series of DOE to derive the optimal cohesive values representing the pull-out experimental test results as accurately as possible. A post-processing code, specifically a Post 26 via APDL, was utilised to process the data. It was possible to automatically obtain the reaction force, displacement and shear stress results at the interface and export them into a text file.

We used a different method to simulate the debonding of KRAIBON® to overcome the convergence challenges connected with the hyperelastic model. The cohesive elements were employed to represent

	τ *average* (MPa)	δ_t (mm)	σ *average* (MPa)	δ_n (mm)	R (-)	α (-)
EP	18	0.04	9	0.04	0.1	1
KR	5.75	0.87	3.5	0.004	0.1	1

Table 2: values of stress and displacement at the last instant of the simulation before interface decohesion.

	$\tau_{average}$ (MPa)	δ_t (mm)	G_t (MPa·mm)	$\sigma_{average}$ (MPa)	δ_n (mm)	G_n (MPa·mm)	R (-)	α (-)
DOE 1	18.3 18 17.7	0.07 0.04 0.01	0.6405 0.63 0.6195 0.366 0.36 0.354 0.0915 0.09 0.0885	8	0.012	0.048	0.13 0.1 0.07	1
DOE 2	35.4 23.6 17.7 14.16 11.8	0.06 0.05 0.04 0.03 0.02	0.354	8	0.012	0.048	0.5 0.1 0.01	1
DOE 3	17.7	0.04	0.354	16 8 4	0.24 0.06 0.024 0.012 0.004	0.96 0.24 0.0964 0.024 0.016	0.1	1

Table 3: DOEs for specimen EP.

both the interface and the behaviour of the elastomer component in place of the hyperelastic model. We modelled the elastomer part as a very stiff material, and the cohesive element properties captured the elastomer deformation. Therefore, the δ_t values, in this case, were an order of magnitude higher.

We divided the parameters optimisation for specimen EP into three DOE (Tab. 3). In the first one, we studied the behaviour as a function of the change in *Mode II* energy by varying τ and δ_t starting from the values found with the bulky FEA (Tab. 2). The value that best represents the G_t of the pull-out test is a value of 0.354 MPa·mm. With this value, the behaviour at the interface was closer to the tests, with a maximum pull-out force around the force that occurs at the plateau. Higher energy values caused a stronger interface and, thus, higher pull-out forces; lower energies induced a weaker interface that did not reach the forces required for the MPT of the free wire. In the second DOE, we changed τ and δ_t but kept G_t constant and equal to the value found in the first DOE. This second step allowed us to optimise the values of τ and δ_t and to optimise the initial stiffness. The final optimal values were 17.7 Mpa for τ and 0.04 mm for δ_t. The third DOE focused on *mode I*, with a change in σ and δ_n, thus a change in *mode I* energy. The optimal value of σ, which allowed for an optimal pull-out force during delamination, is 8 MPa with δ_n of 0.004 m and G_n equal to 0.016 MPa·mm.

For specimen B, the δ_t was set at 1 mm because the CZM needs to simulate the compliance of the elastomer. We derived this value from the experiments and the bulky FEA (Tab. 2). We divided the optimisation into two DOE (Tab. 4). In the first one, we varied R (the ratio between the displacement at maximum τ to δ_t) from 0.1 to 0.85; consequently, the stiffness behaviour also changed. The optimum value that allowed the first linear elastic section to be simulated more faithfully was 0.85. In the second DOE, the τ was varied from 2 to 7 MPa, to search for the value that allows for a maximum pull-out force before delamination as close as possible to the test (i.e., at about 28 N). We found that the optimum value of τ was 6 Mpa; since δ_t is 1 mm, G_t was 3 Mpa*mm.

	(MPa)	(mm)	(MPa·mm)	(MPa)	(mm)	(MPa·mm)	R (-)	α (-)
DOE 1	7	1	3.5	7	0.01	0.035	0.1 0.2 0.3 0.4 0.5 0.6 0.7 0.8 0.85	1
DOE 2	7 6 5 4 3 2	1	3.5 3 2.5 2 1.5 1 0.5	7	0.01	0.035	0.85	1

Table 4: DOEs of specimen KR.

In Fig. 8, we can see the comparison between the FEM and experimental results. We can see a good fitting of the results. In specimen EP, debonding starts after 2 mm of displacement (as in the tests) and progresses at constant force until complete detachment. There is a slight difference in this part since, in the tests, there are phenomena that the simulation could not capture, such as wire interlocking due to debris, and friction.

In specimen KR, there is a difference at the beginning in the linear elastic stretch, which did not change significantly with different CZM parameters. We hypothesised that part of the cause was that the elastomer was characterised only in tension, not in shear or biaxial tension, which could lead to non-negligible differences in behaviour.

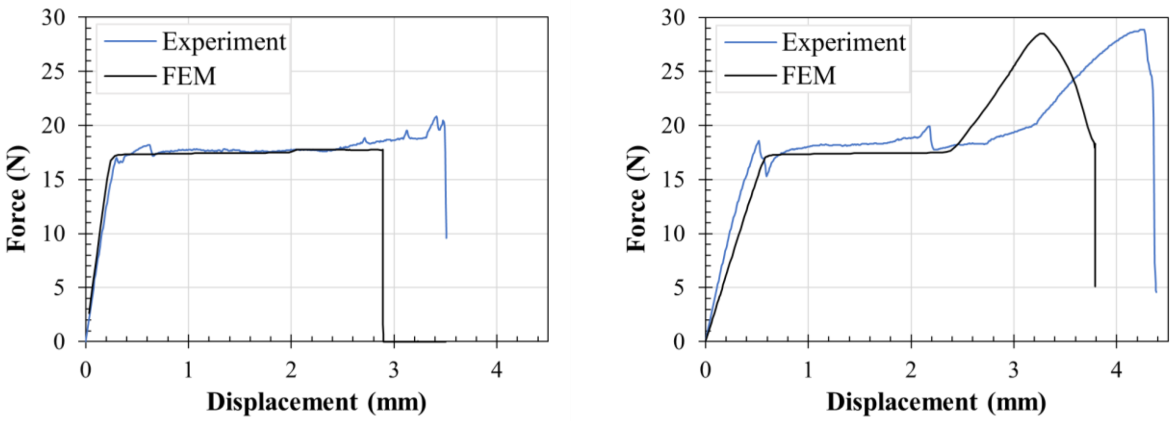

Figure 8: Comparison of force-displacement results of experiment and FEA, of specimen EP (left) and specimen KR (right).

5 SUMMARY AND CONCLUSION

We manufactured specimens with pseudo-elastic shape memory alloy (SMA) wires bonded with either epoxy or KRAIBON®, an elastomeric material. Then, we conducted pull-out tests; the failure mode of all specimens was interfacial decohesion. We observed that the specimens with KRAIBON® had higher bond strength and delayed debonding than those with epoxy. The elastomeric layer accommodated the MPT of the SMA wires without excessive stress concentration, leading to higher force transfer and energy dissipation.

We also performed finite element method (FEM) simulations with bulky to study the stress and strain state in the specimens before debonding. The FEM results agreed with the experimental data, showed the stress distribution, and helped better understand the damage evolution.

To further understand the debonding mechanism, we developed a 2-D FEM model with a CZM to simulate the pull-out test. Based on the experimental results and preliminary simulations, the CZM parameters were optimised with a series of DOE. The FEM-CZM model captured the whole phenomenon of interfacial failure during the pull-out test.

We identified two mechanisms of crack initiation and propagation depending on the matrix material. In the epoxy matrix, large deformations induced by the MPT of the SMA wires caused interfacial debonding and crack propagation. The elastomeric matrix followed the profile variation of the SMA wires during the MPT and maintained adhesion during the test, thanks to the high compliance and maximum strain, which allowed a stress redistribution. This fact enabled KRAIBON® to withstand maximum pull-out forces of about 40 % more than epoxy.

This study demonstrated the advantage of using an elastomer at the SMA-composite interface. The proposed SMAHCs with a KRAIBON® interface offer a simple and effective way to fabricate high-performance smart composites that require high deformability, strength, and shape memory functionality. The proposed CZM can be used to design and engineer smart composites that require high deformability, strength, and shape memory functionality.

The results show the need to investigate the pull-out behaviour on different embedding lengths to understand the phenomena better and validate the CZM for the two interfaces. Moreover, the elastomeric interface can be tailored to suit different applications and loading conditions by varying thickness, stiffness, and adhesion properties. Moreover, the promising results with elastomeric interfaces show the potential for different applications in SMAHCs.

ACKNOWLEDGEMENTS

The authors would like to thank Gummiwerk KRAIBURG GmbH & Co. KG for generously donating the KRAIBON® used in this experiment; and thanks to SAES® for sharing some information about SMA properties.

REFERENCES

[1] C. A. Rogers, C. Liang, and C. R. Fuller, "Modeling of shape memory alloy hybrid composites for structural acoustic control," *J Acoust Soc Am*, vol. 89, no. 1, pp. 210–220, Jan. 1991, doi: 10.1121/1.400503.

[2] J. S. N. Paine and C. A. Rogers, "The Response of SMA Hybrid Composite Materials to Low Velocity Impact," *J Intell Mater Syst Struct*, vol. 5, no. 4, pp. 530–535, Jul. 1994, doi: 10.1177/1045389X9400500409.

[3] Z. Chaudhry and C. A. Rogers, "Response of Composite Beams to an Internal Actuator Force," *Journal of Mechanical Design*, vol. 114, no. 3, pp. 343–348, Sep. 1992, doi: 10.1115/1.2926559.

[4] B. T. Lester, T. Baxevanis, Y. Chemisky, and D. C. Lagoudas, "Review and perspectives: shape memory alloy composite systems," *Acta Mech*, vol. 226, no. 12, pp. 3907–3960, Dec. 2015, doi: 10.1007/s00707-015-1433-0.

[5] K. Jonnalagadda, G. E. Kline, and N. R. Sottos, "Local displacements and load transfer in shape memory alloy composites," *Exp Mech*, vol. 37, no. 1, pp. 78–86, Mar. 1997, doi: 10.1007/BF02328753.

[6] C. Poon, K. Lau, and L. Zhou, "Design of pull-out stresses for prestrained SMA wire/polymer hybrid composites," *Compos B Eng*, vol. 36, no. 1, pp. 25–31, Jan. 2005, doi: 10.1016/j.compositesb.2004.04.002.

[7] S. Rossi, F. Deflorian, A. Pegoretti, D. D'Orazio, and S. Gialanella, "Chemical and mechanical treatments to improve the surface properties of shape memory NiTi wires," *Surf Coat Technol*, vol. 202, no. 10, pp. 2214–2222, 2008, doi: 10.1016/j.surfcoat.2007.09.013.

[8] F. C. Antico, P. D. Zavattieri, and L. G. Hector, "Adhesion of nickel-titanium shape memory alloy wires to polymeric materials: Theory and experiment," *TMS Annual Meeting*, vol. 2, no. June, pp. 563–576, 2012, doi: 10.1002/9781118357002.ch71.

[9] Y. Payandeh, F. Meraghni, E. Patoor, and A. Eberhardt, "Debonding initiation in a NiTi shape memory wire-epoxy matrix composite. Influence of martensitic transformation," *Mater Des*, vol. 31, no. 3, pp. 1077–1084, 2010, doi: 10.1016/j.matdes.2009.09.048.

[10] M. Dawood, M. W. El-Tahan, and B. Zheng, "Bond behavior of superelastic shape memory alloys to carbon fiber reinforced polymer composites," *Compos B Eng*, vol. 77, pp. 238–247, Aug. 2015, doi: 10.1016/j.compositesb.2015.03.043.

[11] M.-W. Han *et al.*, "Woven type smart soft composite for soft morphing car spoiler," *Compos B Eng*, vol. 86, pp. 285–298, Feb. 2016, doi: 10.1016/j.compositesb.2015.10.009.

[12] M. Povolo, T. M. Brugo, and A. Zucchelli, "Numerical and Experimental Investigation of Aluminum/CFRP Hybrid Tubes with Rubber-like Interlayer," *Applied Composite Materials*, vol. 27, no. 3, pp. 269–283, Jun. 2020, doi: 10.1007/s10443-020-09808-4.

[13] T. L. Turner and H. D. Patel, "Analysis of SMA hybrid composite structures in MSC.Nastran and ABAQUS," *J Intell Mater Syst Struct*, vol. 18, no. 5, pp. 435–447, 2007, doi: 10.1177/1045389X06066699.

[14] G. Alfano and M. A. Crisfield, "Finite element interface models for the delamination analysis of laminated composites: mechanical and computational issues," *Int J Numer Methods Eng*, vol. 50, no. 7, pp. 1701–1736, Mar. 2001, doi: 10.1002/nme.93.

[15] H. Lei, Z. Wang, B. Zhou, L. Tong, and X. Wang, "Simulation and analysis of shape memory alloy fiber reinforced composite based on cohesive zone model," *Mater Des*, vol. 40, no. September 2012, pp. 138–147, Sep. 2012, doi: 10.1016/j.matdes.2012.03.037.